Journal of Computational Physics **171,** 227–242 (2001)
doi:10.1006/jcph.2001.6784, available online at http://www.idealibrary.com on IDEAL®

On a Second Order Residual Estimator for Numerical Schemes for Nonlinear Hyperbolic Conservation Laws

Ingo Thomas and Thomas Sonar

Institut für Analysis, Technische Universität Braunschweig, Pockelsstrasse 14, Braunschweig D-38106, Germany
E-mail: i.thomas@tu-bs.de; t.sonar@tu-bs.de

Received January 19, 2000; revised January 18, 2001

We suggest a new technique for the numerical computation of the local residual of nonlinear hyperbolic conservation laws. This techniques relies on a discrete regularization of the numerical data. © 2001 Academic Press

1. INTRODUCTION

Dynamic adaptivity is a very efficient acceleration technique for the numerical solution of nonlinear hyperbolic conservation laws. Recent numerical investigations have shown that adaptivity is able to speed up computations considerably even when fast-moving phenonema dominate [5].

An important question in implementing this technique is what the criterion should be for the refinement or coarsening of control volumes. For many linear equations there are so-called *a posteriori error estimators* available, which allow the control of the local error.

Error control is concerned with the control of the quantity

$$e_h := u_h - u,$$

where u is the exact solution of a problem $\mathcal{L}u = 0$ and u_h denotes a numerical solution. The quantity h refers to a typical length scale in the grid employed for the numerical method. If the operator $\mathcal{L}$ is linear, then $\mathcal{L}e_h = \mathcal{L}u_h - \mathcal{L}u = \mathcal{L}u_h =: r_h$, which connects the error with the computable *residual* r_h. If additionally $\mathcal{L}$ is invertible we immediately get control on the error by means of the residual through

$$e_h = \mathcal{L}^{-1} r_h.$$

Several authors therefore have employed the residual in their constructions of a posteriori refinement indicators; see for example [7–9]. For nonlinear conservation laws, things

0021-9991/01 $35.00

are more complicated. Error estimators exist only for very special cases [13]. Houston, McKenzie, Süli, and Warnecke [6] were the first to provide reliable and efficient a posteriori error indicators for general Petrov–Galerkin methods for Friedrichs systems. In [10] the authors carried over this theory to finite volume approximations of the Euler equations of gas dynamics via a process of symmetrization and linearization. However, reliable and efficient a posteriori error indicators for general nonlinear hyperbolic systems of equations are still not available. Because of this, purely heuristic functionals are often used. A more mathematically based approach is to use the *local residual* as a refinement indicator. An open question is how to make an efficient and accurate numerical approximation of the residual. One reason for this problem lies in the mathematically difficult structure of the ansatz space.

In this paper, we suggest a numerically efficient technique for the approximation of the local residual. Our approach relies on a regularization of the numerical data, which does not destroy the accuracy. The obtained regularity of the data enables us to employ standard techniques of analysis for the approximation of the local residual.

2. CONSERVATION LAWS

We consider a system of m conservation laws on a physical domain $\Omega \subset \mathbf{R}^d$. For a vector-valued, suitably smooth function

$$\mathbf{u} : \Omega \to \mathbf{R}^m$$

a (steady) conservation law is defined through a *flux tensor* $\mathbf{F} = (\mathbf{f}_1, \ldots, \mathbf{f}_d) : \mathcal{D} \subset \mathbf{R}^m \to \mathbf{R}^{m\times d}$ by

$$\operatorname{div} \mathbf{F}(\mathbf{u}) = \sum_{j=1}^{m} \partial_{\mathbf{x}_j} \mathbf{f}_j(\mathbf{u}) = \mathbf{0}, \tag{1}$$

where the $\mathbf{f}_i$ are the *flux functions*. In this paper, we will generally assume that $\mathbf{f}_i \in [\mathrm{C}^2(\mathcal{D}; \mathbf{R}^m)]^d$. Since physically relevant solutions of conservation laws are known to exhibit discontinuities, we define *weak solutions* of the conservation law (1). A function $\mathbf{u} \in [L^\infty(\Omega)]^m$ is a *weak solution* of (1) iff the equation

$$\oint_{\partial\sigma} \mathbf{F}(\mathbf{u}) \otimes \mathbf{n}\, d\mathbf{s} = \mathbf{0}$$

holds on every bounded set (control volume) $\sigma \subset \mathbf{R}^d$, where

$$\mathbf{F} \otimes \mathbf{n} := (\mathbf{f}_1 \cdot \mathbf{n}_1 + \cdots + \mathbf{f}_d \cdot \mathbf{n}_d)$$

and $\mathbf{n}$ denotes the unit outer normal vector at $\partial\sigma$.

We are particularly interested in the solution of the Euler equations of gas dynamics governing inviscid, compressible, steady flow. These equations describe the conservation of mass, momentum, and specific total energy; therefore we have the conserved quantities

$$\mathbf{u} := (\rho, \rho\mathbf{v}, \rho E)^T : \Omega \to \mathbf{R}^m,$$

$m = d + 2$, where ρ is the density, $\mathbf{v}$ is the velocity, and ρE is the specific total energy. The flux functions have the form

$$\mathbf{f}_i(\mathbf{u}) := \left(\rho v_i, \rho v_1 v_i + \delta_1^i p, \ldots, \rho v_d v_i + \delta_d^i p, \rho H v_i\right)^T, \quad i = 1, \ldots, d,$$

where $H = E + \frac{p}{\rho}$ is the *total enthalpy* and δ_k^ℓ denotes the Kronecker delta. Since we have $2 + d$ equations for $3 + d$ unknowns we have to introduce an additional equation of state to close the system. In the case of dry air considered as an ideal gas, the equation of state reads as

$$p = (\kappa - 1)\rho \left(E - \frac{|\mathbf{v}|^2}{2}\right),$$

where $\kappa = 1.4$ denotes the ratio of specific heats.

3. THE FINITE VOLUME METHOD

We give only a short overview of the class of numerical schemes which we employ. Starting from the definition of weak solutions

$$\oint_{\partial\sigma_i} \mathbf{F}(\mathbf{u}) \otimes \mathbf{n}\, d\mathbf{s} = \mathbf{0},$$

we take σ_i to be the boxes (dual grid) of a triangulation. The boundary of each box consists of straight line segments connecting the edge midpoints of edges emanating from node i with the barycentres of the triangles having node i in common; see Fig. 1. Adding an auxiliary time derivative (either to drive to the steady state or to compute unsteady flow) and denoting the indices of neighbouring boxes of σ_i by $\mathcal{N}(i)$ we get

$$\frac{d}{dt}\int_{\sigma_i} \mathbf{u}\, d\mathbf{x} = -\oint_{\partial\sigma_i} \mathbf{F}(\mathbf{u}) \otimes \mathbf{n}\, d\mathbf{s} = -\sum_{j\in\mathcal{N}(i)} \sum_{k=1}^{2} \int_{\iota_{ij}^k} \mathbf{F}(\mathbf{u}) \otimes \mathbf{n}_{ij}^k\, d\mathbf{s}.$$

Denoting by $\overline{\mathbf{u}} := \frac{1}{|\sigma_i|}\int_{\sigma_i} \mathbf{u}\, d\mathbf{x}$ the average of $\mathbf{u}$ over σ_i, employing a Gaussian quadrature rule with n_G points at one segment and introducing an approximate Riemann solver $\mathbf{H}$ then

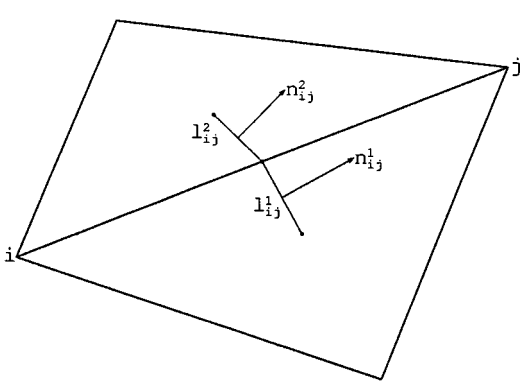

FIG. 1. Boundary of two boxes.

leads to

$$\frac{d}{dt}\bar{\mathbf{U}}_i(t) = -\frac{1}{|\sigma_i|}\sum_{j\in\mathcal{N}(i)}\sum_{k=1}^{2}\frac{|l_{ij}^k|}{2}\sum_{\nu=1}^{n_G}\omega_\nu \mathbf{H}\left(\mathbf{U}_i\left(\mathbf{x}_{ij}^k(s_\nu),t\right),\mathbf{U}_j\left(\mathbf{x}_{ij}^k(s_\nu),t\right);\mathbf{n}_{ij}^k\right).$$

Here, $\mathbf{U}_i$ is a recovery polynomial on σ_i and $\mathbf{x}_{ij}^k(s_\nu)$ denote points on l_{ij}^k with respect to a parametrisation of l_{ij}^k with $s \in [-1, 1]$.

The recovery polynomials are computed in a weighted essentially nonoscillatory manner as described in [1]. With each control volume we associate a stencil containing as many neighbouring control volumes as are necessary for polynomial recovery of a fixed degree. Then a recovery polynomial p_i^k is computed on each stencil k for each conservative variable, and its oscillation behaviour is measured by means of an oscillation indicator, in our case

$$\mathrm{OI}\left(p_i^k\right) := \left\|\nabla p_i^k\right\|_{L^2(\sigma_i)}.$$

According to the oscillation indicator, a weight ω_i^k is defined for the k th recovery polynomial on σ_i so that ω_i^k is large if $\mathrm{OI}(p_i^k)$ is small and vice versa. Additionally, we require $\sum_k \omega_i^k = 1$. For details concerning the construction of the weights see [1]. The final recovery polynomial on σ_i is then defined as

$$\mathbf{U}_i := \sum_k \omega_i^k p_i^k$$

for each of the conservative variables. The resulting schemes for linear and quadratic recovery polynomials are robust, accurate codes which show fairly good convergence behaviour to the steady state. Time-stepping is achieved by means of a TVB–Runge–Kutta scheme.

4. RESIDUAL ESTIMATORS

As we mentioned in the Introduction, we are going to use the residual as an a posteriori error indicator. Let us first summarize some basic facts about this approach.

Ideally, an error indicator should neither underestimate nor overestimate the "true error" $\mathbf{e}_h := \mathbf{u} - \mathbf{u}_h$. In the literature, the first requirement is often referred to as *reliability* and the second one as *efficiency*. By now, reliable error estimates (for nonlinear equations) are available only for scalar equations (see 17). These error estimates, while very interesting, are by no means efficient. In contrast, the efficiency of a residual estimator regarded as an error indicator is almost trivial. Using the integral mean value theorem, we have

$$\|\mathrm{div}\,\mathbf{F}(\mathbf{u}_h)\|_{L^p} = \|\mathrm{div}\,\mathbf{F}(\mathbf{u}_h) - \underbrace{\mathrm{div}\,\mathbf{F}(\mathbf{u})}_{=0}\|_{L^p} \le C\left\{\|\mathbf{e}_h\|_{L^p} + \|\nabla\mathbf{e}_h\|_{L^p}\right\}.$$

By now, we have no reliability results for nonlinear equations.

Let us now discuss the discretization of the residual. As a first guess, one might think of using the finite volume discretization itself for the approximation of the residual. The main problem in this approach is that a finite volume discretization leaves us with discontinuities at the cell faces which have to be taken into account somehow in the calculation of the residual.

This can be done by a sufficiently weak regularity assumption on u_h, namely $u_h \in H^{-1}(\Omega)$. This assumption led us to a H^{-1}-based residual estimator (see Section 5). A rigorous analysis teaches us that the local residual is basically given by the "local total variation" of $\mathbf{F}(\mathbf{u}_h)$. This agrees perfectly with the classical L^1-error estimates for monotone schemes originating in the works of Kruzhkov and Kuznetsow [14, 15]. The result is indeed some sort of a local version of the TVB a priori, respectively. a posteriori, error estimates developed during the past few years by Chanais-Hillairet [16] and Kröner and Ohlberger [17].

But the mathematics behind the approach of a H^{-1}-based estimator seems to be limited to piecewise constant, i.e., first order accurate, data. Therefore, estimators of that type do not recognize that spatial linear data, for instance in an expansion fan, can be captured perfectly Well by a second order scheme on a rather coarse mesh.

It is therefore natural to ask for more accurate residual estimators, i.e., residual estimators that are of the same order of accuracy as the numerical scheme itself. But from our analytical experience H^{-1} feels uncomfortable for doing higher-order approximations, since there is no analog of the approximation theory based on generalized Taylor series. We therefore started to think about a regularization of the numerical data which maps the data into a function space with more structure. We indeed found a rather cheap regularization procedure, which maps the discontinous data, which lie clearly in L^p into the space $W^{1,p}$. We think this regularization is justified for several reasons:

- In the classical theory of analytical solutions for hyperbolic conservation laws, discontinuities appear only on lower-dimensional manifolds; the solution is smooth almost everywhere. Therefore, standard analysis techniques are allowed almost everywhere in the physical domain.
- $W^{1,p}$ is dense in L^p. Hence, for any discontinous piecewise polynomial, numerical approximation u_h, and any given $\varepsilon > 0$, there exists a $u_h^* \in W^{1,p}$ such that

$$\|u_h - u_h^*\|_{L^p} \leq \varepsilon \leq h^2.$$

There is therefore a $W^{1,p}$ approximation of the numerical data which lies within the accuracy of the numerical scheme.

5. H^{-1}-BASED RESIDUAL ESTIMATOR

In [11] and [12] Sonar and Warnecke developed an error indicator within the framework of piecewise constant functions, i.e., working immediately with the cell averages of finite volume schemes *without* regularizing the data. On cell σ_i with neighbours σ_j, $j \in \mathcal{N}(i)$, consider data $\mathbf{U}_h$ being constant on the σ_ks and let $|[\mathbf{F}(\mathbf{U}_h) \otimes \mathbf{n}_{ij}]_{\partial\sigma_i \cap \partial\sigma_j}|$ denote the jump of the normal fluxes $\mathbf{F}(\mathbf{U}_h) \otimes \mathbf{n}_{ij}$ across the edge $\partial\sigma_i \cap \partial\sigma_j$. The quantity

$$\eta_{\sigma i}^h := \max_{j \in \mathcal{N}(i)} \left\{ \left| [\mathbf{F}(\mathbf{U}_h) \otimes \mathbf{n}_{ij}]_{\partial\sigma_i \cap \partial\sigma_j} \right| \cdot |\sigma_i \cap \sigma_j| \right\}$$

then measures the largest jump of the normal fluxes across the edges of the cell σ_i weighted with the length of the edges. Considering larger patches Σ_{loc} of cells we are able to compute

$$\eta_{\Sigma_{\text{loc}}}^h := \left(\sum_{\sigma_i \in \Sigma_{\text{loc}}} \left| \eta_{\sigma_i}^h \right|^2 \right)^{1/2},$$

and it was shown in [11] that there are constants C, C′ > 0 independent of h such that

$$C'\eta^h_{\Sigma_{\text{loc}}} \le \|\operatorname{div}\mathbf{F}(\mathbf{u}_h)\|_{H^{-1}(\Sigma_{\text{loc}})} \le C\eta^h_{\Sigma_{\text{loc}}},$$

i.e., $\eta^h_{\Sigma_{\text{loc}}}$ is an estimator for the H^{-1}-norm of the residual. It is this finite difference estimator that will be used for comparison purposes in the sequel.

6. DISCRETE REGULARIZATION OF THE DATA

The finite volume method described above leaves us with piecewise constant data on each control volume. Let $S^1_h(\Omega)$ denote the space of piecewise, linear, discontinuous functions on the boxes σ_i, which form a partition of the computational domain Ω. We are interested in the construction of a *discrete* regularization operator

$$R : S^1_h(\Omega) \to W^{1,p}(\Omega) \tag{2}$$

which does not destroy the accuracy of the data. Since the $S^1_h(\Omega)$ data is second order accurate in the absence of shocks, R has to satisfy the property (note that $S^1_h(\Omega) \subset L^p(\Omega)$)

$$\|u_h - Ru_h\|_{L^p}(\Omega) = \mathcal{O}(h^2) \tag{3}$$

in smooth regions.

We describe the construction of the discrete regularization R only for the interior of the physical domain Ω. For each control volume σ, we choose a point $\mathbf{x}_\sigma$ in the interior $\mathring{\sigma}$ of σ. In the interior of Ω there exists always a simplicial decomposition Λ_h of Ω such that each $\mathbf{x}_\sigma$ is a node of Λ_h. We refer to that decomposition as the *dual mesh*. By evaluating the ansatz functions u_σ in the points $\mathbf{x}_\sigma$, we obtain $(d+1)\times m$-dimensional information on each cell of the dual mesh. This is exactly the required information for a linear interpolation on the simplex. The continuity of the interpolation can be seen as follows: The interpolation of the data at a face of a simplex depends only on the data of the vertices of the face; it is in fact the linear interpolation of the data on the face. The new interpolation is a continuous second order interpolation of the point values $u(\mathbf{x}_\sigma)$. Therefore, the accuracy condition (3) holds whenever there is no shock front separating the data points.

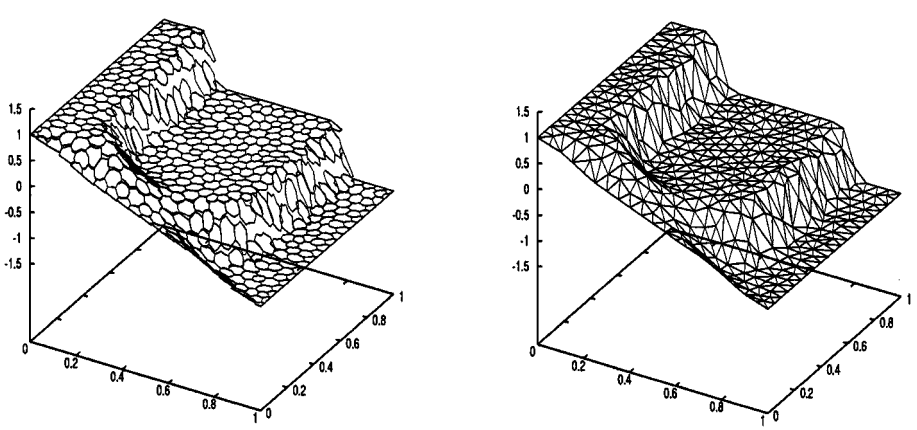

FIG. 2. Left: piecewise polynomial, discontinuous data. Right: piecewise polynomial, continuous data.

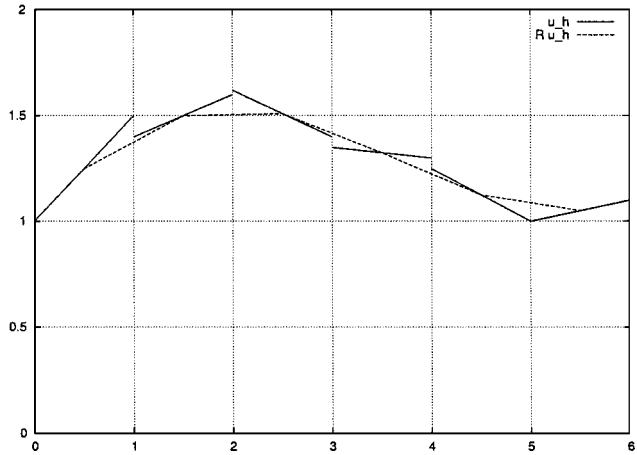

FIG. 3. Solid line: given S_h^1 data. Dashed line: dual H^1 data.

The one-dimensional case is almost self-explanatory. In Fig. 3 we always choose $\mathbf{x}_\sigma$ to be the midpoint of σ; we evaluate the linear function on σ in $\mathbf{x}_\sigma$ and connect the obtained point values by linear interpolation.

A particularly simple two-dimensional case is the box-grid. In the interior of the domain, each vertex of the underlying triangulation lies in the interior of its box, and each box contains exactly one vertex of the underlying triangulation. Therefore, the underlying triangulation itself is a *dual mesh*. We simply have to evaluate the ansatz functions in the vertices of the underlying triangulation and calculate the linear interpolation on each triangle as shown in Fig. 2.

For a cartesian, nonconforming grid, we again chose $\mathbf{x}_\sigma$ as the centers of the cells. We decompose the domain into triples of cells as shown in Fig. 4.

7. H^1-BASED RESIDUAL ESTIMATOR

In this section we will derive formulae for the actual calculation of the norm of the residual of the regularized data $\mathbf{u}_h^* := R\,\mathbf{u}_h$.

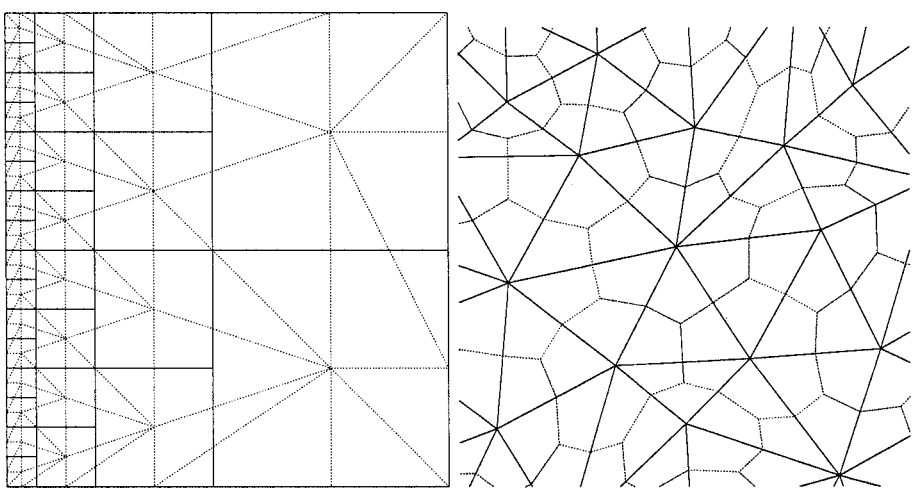

FIG. 4. Left: Cartesian, nonconforming grid and dual mesh. Right: box-grid and dual mesh.

Since our data lie in $W^{1,p}(\Omega)$ for any p, we are free to choose any L^p norm of the residual. From a purely mathematical point of view, the most natural norm would be L^1, since BV (which is, so to speak, the subspace of L^1 with finite residual) is the space of solutions the scalar equations are known to live in.

But the L^1-norm is difficult to obtain numerically, since its calculation requires a subdivision of the control volumes depending on the sign of the data. We therefore chose the L^2-norm of the residual instead. Since we are from now on only concerned with the regularized data, we suppress the star and set $\mathbf{u}_h = \mathbf{u}_h^*$.

Our objective is a numerical algorithm for a second order approximation of the local residual, i.e., we want to approximate the quantity

$$r(\mathbf{u}_h) := \|\operatorname{div} \mathbf{F}(\mathbf{u}_h)\|_{L^2(\sigma)}.$$

This turns out to be a tedious, but straightforward task. We first give the formulae for a d-dimensional system of m equations, and afterwards we describe the case of a general scalar system and the system of the Euler equations in two space dimensions.

Since the resulting formulae in the case of systems tend to be quite complicated, we introduce the shorthand notations of the Jacobian $\nabla_{\boldsymbol{u}} \mathbf{f}_k \in \mathrm{C}^1(\mathbf{R}^m; \mathbf{R}^{m\times m})$ of a flux function and set $\mathbf{x}^\alpha := \Pi_{j=1}^d x_j^{\alpha_j}$.

We have

$$\operatorname{div} \mathbf{F}(\mathbf{u}_h) = \partial_{x_1} \mathbf{f}_1(\mathbf{u}_h) + \cdots + \partial_{x_d} \mathbf{f}_d(\mathbf{u}_h).$$

A Taylor expansion of one term in this sum reveals[1]

$$\begin{aligned}
\partial_{x_j} \mathbf{f}_j(\mathbf{u}_h(\mathbf{x})) &= \nabla_{\mathbf{u}} \mathbf{f}_j(\mathbf{u}_h(\mathbf{x})) \cdot \underbrace{\partial_{x_j} \mathbf{u}_h}_{=\text{const on } \sigma} \\
&= \left\{ \nabla_{\mathbf{u}} \mathbf{f}_j \cdot \partial_{x_j} \mathbf{u}_h \right\}(\mathbf{u}_h(\mathbf{x}_0) + (\mathbf{x} - \mathbf{x}_0) \nabla_{\mathbf{x}} \mathbf{u}_h) = \left\{ \nabla_{\mathbf{u}} \mathbf{f}_j \cdot \partial_{x_j} \mathbf{u}_h \right\}(\mathbf{u}(\mathbf{x}_0)) \\
&\quad + \nabla_{\mathbf{u}} \left\{ \nabla_{\mathbf{u}} \mathbf{f}_j \cdot \partial_{x_j} \mathbf{u}_h \right\}(\mathbf{u}(\mathbf{x}_0)) \cdot (\mathbf{x} - \mathbf{x}_0) \cdot \nabla_{\mathbf{x}} \mathbf{u}_h \\
&\quad + \mathcal{O}\left(\|\mathbf{x} - \mathbf{x}_0\|_2^2 \, \|\nabla_{\mathbf{x}} \mathbf{u}_h\|_2^2 \right)
\end{aligned} \tag{4}$$

Rewriting the latter formula in matrix notation and abbreviating $\mathbf{h} = \mathbf{x} - \mathbf{x}_0$ and $\mathbf{u}_0 = \mathbf{u}_h(\mathbf{x}_0)$ we get

$$\begin{aligned}
\partial_{x_j} \mathbf{f}_j(\mathbf{u}_h(\mathbf{x})) = &\begin{bmatrix} \sum_{k=1}^m \partial_{u_k} f_{j,1}(\mathbf{u})|_{\mathbf{u}=\mathbf{u}_0} \cdot \partial_{x_j} u_{h,k} \\ \vdots \\ \sum_{k=1}^m \partial_{u_k} f_{j,m}(\mathbf{u})|_{\mathbf{u}=\mathbf{u}_0} \cdot \partial_{x_j} u_{h,k} \end{bmatrix} \\
&+ \begin{bmatrix} \sum_{\ell=1}^m \left[\left(\sum_{k=1}^d \partial_{x_k} u_{h,\ell} \cdot h_k \right) \cdot \left(\sum_{k=1}^m \partial_{u_\ell} \partial_{u_k} f_{j,1}(\mathbf{u})|_{\mathbf{u}=\mathbf{u}_0} \cdot \partial_{x_j} u_{h,k} \right) \right] \\ \vdots \\ \sum_{\ell=1}^m \left[\left(\sum_{k=1}^d \partial_{x_k} u_{h,\ell} \cdot h_k \right) \cdot \left(\sum_{k=1}^m \partial_{u_\ell} \partial_{u_k} f_{j,m}(\mathbf{u})|_{\mathbf{u}=\mathbf{u}_0} \cdot \partial_{x_j} u_{h,k} \right) \right] \end{bmatrix} \\
&+ \mathcal{O}(\|\mathbf{h}\|^2).
\end{aligned}$$

[1] Note that due to the linearity of the ansatz function $\mathbf{u}_h$, we have $\nabla_x \mathbf{u}_h(\mathbf{x}) = \text{const} =: \nabla_x \mathbf{u}_h$.

Using these formulae, we have a second order approximation of the components of the residual given by the linear polynomial

$$\sum_{j=1}^{d} \partial_{x_j} f_{j,k}(\mathbf{u}_h) = \sum_{|\alpha|\le 1} a_{\alpha,k}\, \mathbf{h}^{\alpha} + \mathcal{O}\big(\|\mathbf{h}\|_2^2\big)$$

with multiindex $\alpha = (\alpha_1, \ldots, \alpha_d)$. We obtain the L^2-norm of the estimator straightforwardly as

$$\int_{\sigma} \left(\sum_{|\alpha|\le 1} a_{\alpha,k}\, \mathbf{h}^{\alpha} \right)^2 d\mathbf{h} = \sum_{|\alpha+\beta|\le 2} a_{\alpha,k}\, a_{\beta,k}\, I_{\alpha+\beta} \qquad \text{with } I_{\alpha} := \int_{\sigma} \mathbf{h}^{\alpha}\, d\mathbf{h}. \tag{5}$$

Note that only $\boldsymbol{a}_{\alpha}$ depends on the data; the integrals I_{α} may be precomputed.

The remaining task is to calculate the a_{α}, which depend on the differential operator as well as the actual data. The a_{α} consist of the derivatives of the flux function

$$\nabla_{\mathbf{u}} \mathbf{f}_j(\mathbf{u}_h(\mathbf{x}_0)) \cdot \partial_{x_j} \mathbf{u}_h(\mathbf{x}_0) \qquad \text{and} \qquad \nabla_{\mathbf{u}} \big\{ \nabla_{\mathbf{u}} \mathbf{f}_j(\mathbf{u}_h(\mathbf{x}_0)) \cdot \partial_{x_j} \mathbf{u}_h \big\} \cdot \partial_{x_k} \mathbf{u}_h$$

as computed in the Taylor expansion above. In many papers on a posteriori error estimation, the importance of the scaling factor of the adaption indicator is emphasized [8, 11]. It has been pointed out that the scaling has to decrease at least linearly with the diameter of the h of a control volume. This is a first criterion for our residual estimator. Luckily, this criterion is consistent with that requirement, since the components $a_{\alpha} \in \mathcal{O}(1)$ are scaled with $h^{|\alpha|+1}$.

As discussed above, the residual estimator should be of the same order of accuracy as the numerical scheme. Since we have third and even fourth order accurate weighted essentially nonoscillatory (WENO) schemes [1, 3], it would be desirable to have residual estimators of the same accuracy. But there are a number of difficulties here.

- It is the authors' belief that one has to leave the framework of piecewise polynomials in order to achieve more regularity than $W^{1,p}$. One could of course think of a radial-basis-function ansatz or something similar; but this would not fit into a finite volume framework as nicely as the second order approach described here.
- A higher order polynomial ansatz seems to increase the noise in the numerical residual distribution. This seems to be due to the fact that the calculation of the leading coefficients of a higher order polynomial is significantly more ill-conditioned than in the linear case (a similar effect had been observed for the third order WENO recovery algorithm itself; see 2).

7.1. The Two-Dimensional Scalar Equation

In order to illustrate the considerations above, we study a scalar equation in two space dimensions,

$$\operatorname{div}(f(u_h), g(u_h)) = 0.$$

For this equation, the formulae of the last section read as

$$\operatorname{div}(f(u_h), g(u_h)) = \sum_{|\alpha|\le 1} a_{\alpha} \mathbf{h}^{\alpha} + \mathcal{O}(\|\mathbf{h}\|_2)$$

with

$$
\begin{aligned}
a_{(0,0)} &= \partial_u f(u_h) \cdot \partial_x u_h + \partial_u g(u_h) \cdot \partial_y u_h \\
a_{(1,0)} &= \partial_{uu} f(u_h) \cdot (\partial_x u_h)^2 + \partial_{uu} g(u_h) \cdot \partial_x u_h \cdot \partial_y u_h \\
a_{(0,1)} &= \partial_{uu} f(u_h) \cdot \partial_x u_h \cdot \partial_y u_h + \partial_{uu} g(u_h) \cdot (\partial_y u_h)^2.
\end{aligned}
$$

Using these quantities, we may calculate the residual on simplex σ as

$$
\begin{aligned}
r(u_h)^2 = a_{(0,0)}|\sigma| + 2\, a_{(0,0)}\, a_{(1,0)} \int_\sigma h_1 \, d\mathbf{h} + 2\, a_{(0,0)}\, a_{(0,1)} \int_\sigma h_2 \, d\mathbf{h} + 2\, a_{(1,0)}\, a_{(0,1)} \\
\times \int_\sigma h_1 h_2 \, d\mathbf{h} + a_{(1,0)}^2 \int_\sigma h_1^2 \, d\mathbf{h} + a_{(0,1)}^2 \int_\sigma h_2^2 \, d\mathbf{h} + \mathcal{O}(\|\mathbf{h}\|^2)|\sigma|.
\end{aligned}
$$

7.2. The Steady Two-Dimensional Euler Equations

According to our considerations above, we have to calculate first and second derivatives of the flux tensor

$$
\mathbf{F} \circ \mathbf{u} := \begin{bmatrix} \rho v_1 & \rho v_2 \\ \rho v_1^2 + p & \rho v_1 v_2 \\ \rho v_1 v_2 & \rho v_2^2 + p \\ \rho H v_1 & \rho H v_2 \end{bmatrix},
$$

where $\mathbf{u} := (\rho, \rho v_1, \rho v_2, \rho E)^T$. Since this is a tedious and error-prone task to do manually, we computed the quantities necessary for our residual estimator with the computer algebra package *Mathematica*. The results of the automated calculation are presented in Fig. 5.

8. NUMERICAL EXAMPLES

8.1. A Two-Dimensional Scalar Equation

Consider the scalar equation

$$
\begin{aligned}
u_t + u u_x + u_y &= 0 \qquad\qquad \text{on } \Omega := [0,1]^2 \\
u(x, y, 0) &= 0 \\
u &= 1 - 2x \quad \text{on } \partial\Omega.
\end{aligned} \tag{6}
$$

The steady solution of this equation can be constructed by the method of characteristics. The characteristic equations are given by $dy/ds = 1$, $dx/ds = u$, or $dy/dx = 1/u$. Assuming the given boundary data, the leftmost characteristic g_1 is given by x, and the rightmost characteristic g_2 is given by $1 - x$ (see Fig. 6. The characteristics meet at point P, where the shock g_3 starts. The Rankine–Hugoniot condition yields the shock slope $dx/dy = 0$.

The data at point Q lie on the characteristic connecting the point P and PQ; therefore $u(P) = u(PQ)$ holds.

Knowing the analytical solution enables us to calculate the exact error $e_h = u - u_h$; therefore, we can compare the actual error and the residual estimator.

$\left(\nabla_{\boldsymbol{u}} \boldsymbol{f}_1(\boldsymbol{u}_h) \cdot \partial^{(1,0)} \boldsymbol{u}_h\right)_1$	$(\rho u)_{(1,0)}$
$\left(\nabla_{\boldsymbol{u}} \boldsymbol{f}_1(\boldsymbol{u}_h) \cdot \partial^{(1,0)} \boldsymbol{u}_h\right)_2$	$(-1+\kappa)\,(\rho E)_{(1,0)} + (3-\kappa)\,(\rho u)_{(1,0)}\,u + (1-\kappa)\,(\rho v)_{(1,0)}\,v + \frac{\rho_{(1,0)}\left(-3\,u^2+\kappa\,u^2-v^2+\kappa\,v^2\right)}{2}$
$\left(\nabla_{\boldsymbol{u}} \boldsymbol{f}_1(\boldsymbol{u}_h) \cdot \partial^{(1,0)} \boldsymbol{u}_h\right)_3$	$(\rho v)_{(1,0)}\,u + (\rho u)_{(1,0)}\,v - \rho_{(1,0)}\,u\,v$
$\left(\nabla_{\boldsymbol{u}} \boldsymbol{f}_1(\boldsymbol{u}_h) \cdot \partial^{(1,0)} \boldsymbol{u}_h\right)_4$	$\kappa\,(\rho E)_{(1,0)}\,u + (1-\kappa)\,(\rho v)_{(1,0)}\,u\,v + \frac{(\rho u)_{(1,0)}\left(2\,E\,\kappa+3\,u^2-3\,\kappa\,u^2+v^2-\kappa\,v^2\right)}{2} + \rho_{(1,0)}\,u\,\left(-(E\,\kappa)+(\kappa-1)(u^2+v^2)\right)$
$\left(\nabla_{\boldsymbol{u}} \boldsymbol{f}_2(\boldsymbol{u}_h) \cdot \partial^{(0,1)} \boldsymbol{u}_h\right)_1$	$(\rho v)_{(0,1)}$
$\left(\nabla_{\boldsymbol{u}} \boldsymbol{f}_2(\boldsymbol{u}_h) \cdot \partial^{(0,1)} \boldsymbol{u}_h\right)_2$	$(\rho v)_{(0,1)}\,u + (\rho u)_{(0,1)}\,v - \rho_{(0,1)}\,u\,v$
$\left(\nabla_{\boldsymbol{u}} \boldsymbol{f}_2(\boldsymbol{u}_h) \cdot \partial^{(0,1)} \boldsymbol{u}_h\right)_3$	$(-1+\kappa)\,(\rho E)_{(0,1)} + (1-\kappa)\,(\rho u)_{(0,1)}\,u + (3-\kappa)\,(\rho v)_{(0,1)}\,v + \frac{\rho_{(0,1)}\left(-u^2+\kappa\,u^2-3\,v^2+\kappa\,v^2\right)}{2}$
$\left(\nabla_{\boldsymbol{u}} \boldsymbol{f}_2(\boldsymbol{u}_h) \cdot \partial^{(0,1)} \boldsymbol{u}_h\right)_4$	$\kappa\,(\rho E)_{(0,1)}\,v + (1-\kappa)\,(\rho u)_{(0,1)}\,u\,v + \frac{(\rho v)_{(0,1)}\left(2\,E\,\kappa+u^2-\kappa\,u^2+3\,v^2-3\,\kappa\,v^2\right)}{2} + \rho_{(0,1)}\,v\,\left(-(E\,\kappa)-u^2+\kappa\,u^2-v^2+\kappa\,v^2\right)$
$\left(\nabla_{\boldsymbol{u}}(\nabla_{\boldsymbol{u}} \boldsymbol{f}_1(\boldsymbol{u}_h) \cdot \partial^{(1,0)} \boldsymbol{u}_h) \cdot \partial^{\alpha} \boldsymbol{u}_h\right)_1$	0
$\left(\nabla_{\boldsymbol{u}}(\nabla_{\boldsymbol{u}} \boldsymbol{f}_1(\boldsymbol{u}_h) \cdot \partial^{(1,0)} \boldsymbol{u}_h) \cdot \partial^{\alpha} \boldsymbol{u}_h\right)_2$	$\frac{(-3+\kappa)\,(\rho u)_{\underline{\alpha}}\left(-(\rho u)_{(1,0)}+\rho_{(1,0)}\,u\right)}{\rho} + \frac{(-1+\kappa)\,(\rho v)_{\underline{\alpha}}\left(-(\rho v)_{(1,0)}+\rho_{(1,0)}\,v\right)}{\rho} + \rho_{\underline{\alpha}}\left(\frac{(-3+\kappa)\,(\rho u)_{(1,0)}\,u}{\rho} + \frac{(-1+\kappa)\,(\rho v)_{(1,0)}\,v}{\rho} + \frac{\rho_{(1,0)}\left(3\,u^2-\kappa\,u^2+v^2-\kappa\,v^2\right)}{\rho}\right)$
$\left(\nabla_{\boldsymbol{u}}(\nabla_{\boldsymbol{u}} \boldsymbol{f}_1(\boldsymbol{u}_h) \cdot \partial^{(1,0)} \boldsymbol{u}_h) \cdot \partial^{\alpha} \boldsymbol{u}_h\right)_3$	$\frac{(\rho u)_{\underline{\alpha}}\,(\rho v)_{(1,0)}+(\rho u)_{(1,0)}\,(\rho v)_{\underline{\alpha}}-(\rho v)_{\underline{\alpha}}\,\rho_{(1,0)}\,u-(\rho v)_{(1,0)}\,\rho_{\underline{\alpha}}\,u-(\rho u)_{\underline{\alpha}}\,\rho_{(1,0)}\,v-(\rho u)_{(1,0)}\,\rho_{\underline{\alpha}}\,v+2\,\rho_{(1,0)}\,\rho_{\underline{\alpha}}\,u\,v}{\rho}$
$\left(\nabla_{\boldsymbol{u}}(\nabla_{\boldsymbol{u}} \boldsymbol{f}_1(\boldsymbol{u}_h) \cdot \partial^{(1,0)} \boldsymbol{u}_h) \cdot \partial^{\alpha} \boldsymbol{u}_h\right)_4$	$\frac{\kappa\,(\rho E)_{\underline{\alpha}}\left((\rho u)_{(1,0)}-\rho_{(1,0)}\,u\right)}{\rho} + \frac{(-1+\kappa)\,(\rho v)_{\underline{\alpha}}\left(-\left((\rho v)_{(1,0)}\,u\right)-(\rho u)_{(1,0)}\,v+2\,\rho_{(1,0)}\,u\,v\right)}{\rho} + \frac{(\rho u)_{\underline{\alpha}}\left(\kappa\,(\rho E)_{(1,0)}-E\,\kappa\,\rho_{(1,0)}+3\,(\rho u)_{(1,0)}\,u-3\,\kappa\,(\rho u)_{(1,0)}\,u-3\,\rho_{(1,0)}\,u^2+3\,\kappa\,\rho_{(1,0)}\,u^2+(\rho v)_{(1,0)}\,v-\kappa\,(\rho v)_{(1,0)}\,v-\rho_{(1,0)}\,v^2+\kappa\,\rho_{(1,0)}\,v^2\right)}{\rho} + \frac{\rho_{\underline{\alpha}}\left(-\left(E\,\kappa\,(\rho u)_{(1,0)}\right)-\kappa\,(\rho E)_{(1,0)}\,u+2\,e\,\kappa\,\rho_{(1,0)}\,u-3\,(\rho u)_{(1,0)}\,u^2+3\,\kappa\,(\rho u)_{(1,0)}\,u^2\right)}{\rho} + \frac{\left(3\,\rho_{(1,0)}\,u^3-3\,\kappa\,\rho_{(1,0)}\,u^3-2\,(\rho v)_{(1,0)}\,u\,v+2\,\kappa\,(\rho v)_{(1,0)}\,u\,v-(\rho u)_{(1,0)}\,v^2+\kappa\,(\rho u)_{(1,0)}\,v^2+3\,\rho_{(1,0)}\,u\,v^2-3\,\kappa\,\rho_{(0,1)}\,u\,v^2\right)}{\rho}$
$\left(\nabla_{\boldsymbol{u}}(\nabla_{\boldsymbol{u}} \boldsymbol{f}_2(\boldsymbol{u}_h) \cdot \partial^{(0,1)} \boldsymbol{u}_h) \cdot \partial^{\alpha} \boldsymbol{u}_h\right)_1$	0
$\left(\nabla_{\boldsymbol{u}}(\nabla_{\boldsymbol{u}} \boldsymbol{f}_2(\boldsymbol{u}_h) \cdot \partial^{(0,1)} \boldsymbol{u}_h) \cdot \partial^{\alpha} \boldsymbol{u}_h\right)_2$	$\frac{(-3+\kappa)\,(\rho u)_{\underline{\alpha}}\left(-(\rho u)_{(0,1)}+\rho_{(0,1)}\,u\right)}{\rho} + \frac{(-1+\kappa)\,(\rho v)_{\underline{\alpha}}\left(-(\rho v)_{(0,1)}+\rho_{(0,1)}\,v\right)}{\rho} + \rho_{\underline{\alpha}}\left(\frac{(-3+\kappa)\,(\rho u)_{(0,1)}\,u}{\rho} + \frac{(-1+\kappa)\,(\rho v)_{(0,1)}\,v}{\rho} + \frac{\rho_{(0,1)}\left(3\,u^2-\kappa\,u^2+v^2-\kappa\,v^2\right)}{\rho}\right)$
$\left(\nabla_{\boldsymbol{u}}(\nabla_{\boldsymbol{u}} \boldsymbol{f}_2(\boldsymbol{u}_h) \cdot \partial^{(0,1)} \boldsymbol{u}_h) \cdot \partial^{\alpha} \boldsymbol{u}_h\right)_3$	$\frac{(\rho u)_{\underline{\alpha}}\,(\rho v)_{(0,1)}+(\rho u)_{(0,1)}\,(\rho v)_{\underline{\alpha}}-(\rho v)_{\underline{\alpha}}\,\rho_{(0,1)}\,u-(\rho v)_{(0,1)}\,\rho_{\underline{\alpha}}\,u-(\rho u)_{\underline{\alpha}}\,\rho_{(0,1)}\,v-(\rho u)_{(0,1)}\,\rho_{\underline{\alpha}}\,v+2\,\rho_{(0,1)}\,\rho_{\underline{\alpha}}\,u\,v}{\rho}$
$\left(\nabla_{\boldsymbol{u}}(\nabla_{\boldsymbol{u}} \boldsymbol{f}_2(\boldsymbol{u}_h) \cdot \partial^{(0,1)} \boldsymbol{u}_h) \cdot \partial^{\alpha} \boldsymbol{u}_h\right)_4$	$\frac{\kappa\,(\rho E)_{\underline{\alpha}}\left((\rho u)_{(0,1)}-\rho_{(0,1)}\,u\right)}{\rho} + \frac{(-1+\kappa)\,(\rho v)_{\underline{\alpha}}\left(-\left((\rho v)_{(0,1)}\,u\right)-(\rho u)_{(0,1)}\,v+2\,\rho_{(0,1)}\,u\,v\right)}{\rho} + \frac{(\rho u)_{\underline{\alpha}}\left(\kappa\,(\rho E)_{(0,1)}-E\,\kappa\,\rho_{(0,1)}+3\,(\rho u)_{(0,1)}\,u-3\,\kappa\,(\rho u)_{(0,1)}\,u-3\,\rho_{(0,1)}\,u^2+3\,\kappa\,\rho_{(0,1)}\,u^2+(\rho v)_{(0,1)}\,v-\kappa\,(\rho v)_{(0,1)}\,v-\rho_{(0,1)}\,v^2+\kappa\,\rho_{(0,1)}\,v^2\right)}{\rho} + \frac{\rho_{\underline{\alpha}}\left(-\left(E\,\kappa\,(\rho u)_{(0,1)}\right)-\kappa\,(\rho E)_{(0,1)}\,u+2\,e\,\kappa\,\rho_{(0,1)}\,u-3\,(\rho u)_{(0,1)}\,u^2+3\,\kappa\,(\rho u)_{(0,1)}\,u^2\right)}{\rho} + \frac{\left(3\,\rho_{(0,1)}\,u^3-3\,\kappa\,\rho_{(0,1)}\,u^3-2\,(\rho v)_{(0,1)}\,u\,v+2\,\kappa\,(\rho v)_{(0,1)}\,u\,v-(\rho u)_{(0,1)}\,v^2+\kappa\,(\rho u)_{(0,1)}\,v^2+3\,\rho_{(0,1)}\,u\,v^2-3\,\kappa\,\rho_{(0,1)}\,u\,v^2\right)}{\rho}$

FIG. 5. First and second order derivatives of the Euler operator.

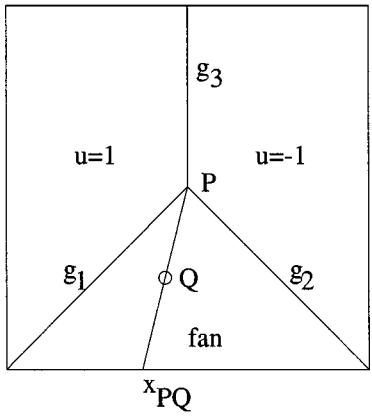

FIG. 6. Construction of the steady solution.

We solved Eq. (6) with a second order finite volume solver on an isotropic grid with about 6500 control volumes (see Fig. 7).

We compared the residual information of the H^{-1}-residual estimator and the information of the H^1-residual estimator in Fig. 8.

Since it would be difficult to compute the L^2-norm of the exact error $e_h = u - u_h$ numerically, we projected the steady numerical solution onto a finer subgrid with roughly 50,000 control volumes. On this fine grid, we calculated a second order approximation of the local L^2-norm. The isolines of $\|e_h\|_2$ are plotted in Fig. 9. We observe that the influence of the asymmetric geometry of the grid is enforced by a first order error indicator compared to the true error, whereas the second order indicator seems to provide the correct amount of geometry dependency.

8.2. The Steady Two-Dimensional Euler Equations

Consider the standard test case of flow around a NACA0012 profile with Mach number $Ma = 0.8$ and angle of attack $\alpha = 1.25$ on a box-grid with 8510 cells as shown in Fig. 10. In Fig. 11, we compare the isolines of the H^1-residual estimator with the isolines of the

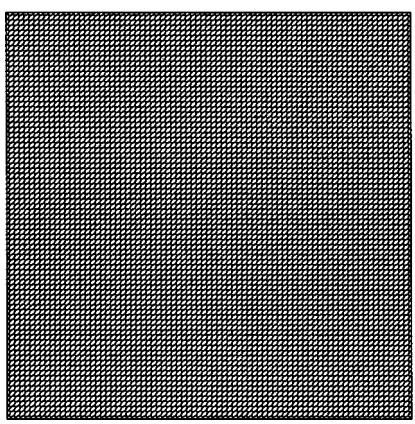

FIG. 7. Computational mesh for the scalar example.

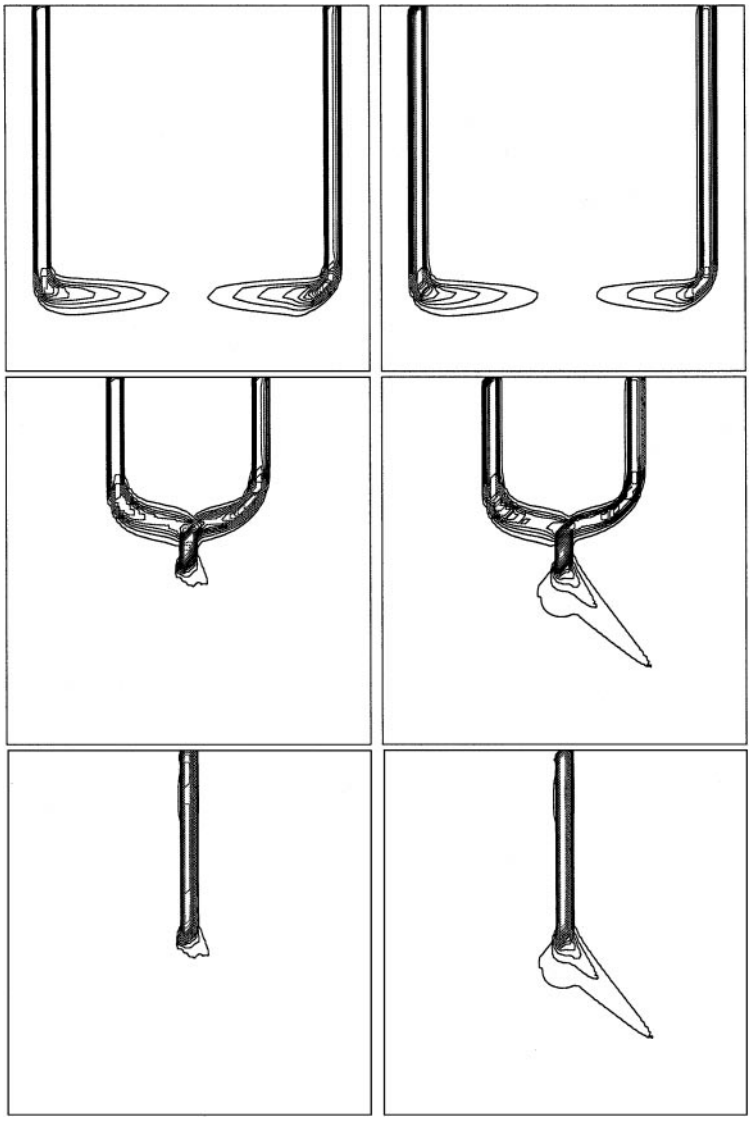

FIG. 8. Left: isolines of H^{-1} residual estimator (min 0, delta 0.02). Right: isolines of H^1-residual estimator (min 0, delta 0.003).

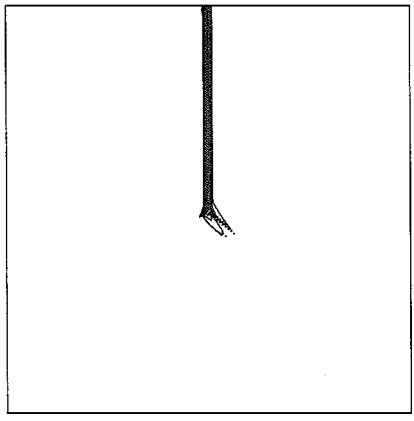

FIG. 9. Isolines of the actual error of the numerical solution (min 0, delta 4e-6).

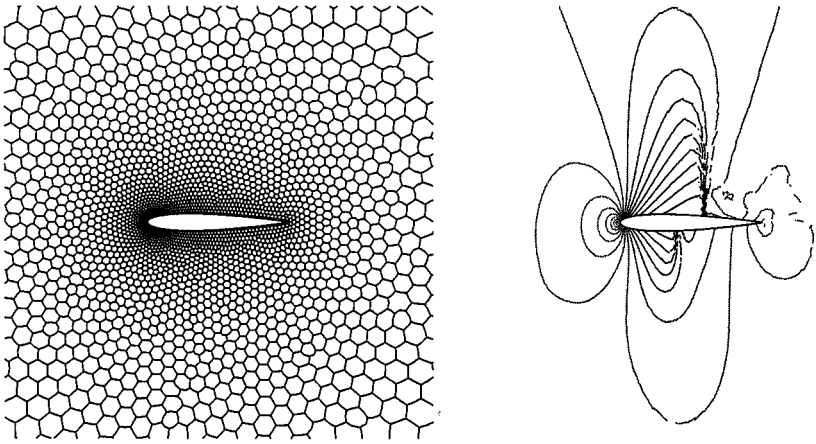

FIG. 10. Grid and steady density distribution.

H^{-1}-residual estimator for the steady state solution given on a fixed grid. We observe quite different qualitative behaviour: the H^1-residual estimator nearly vanishes in the smooth regions of the flow, whereas the H^{-1}-residual estimator produces noise in the smooth regions proportional to the local gradients of the data.

8.3. Generalization to Unsteady Flow

As a final example we generalize our indicator to unsteady flows. Only the spatial residual is computed, and the residual due to the time-stepping is not taken into account. The example chosen is the forward-facing step of Woodward and Colella [18] where a Mach 3 flow starts at time $t = 0$. Shown in Fig. 12 is the control volume grid and the corresponding density distribution at time $t = 8$. The new indicator is not only capable of resolving the shocks but also refines the contact discontinuity and the corner point.

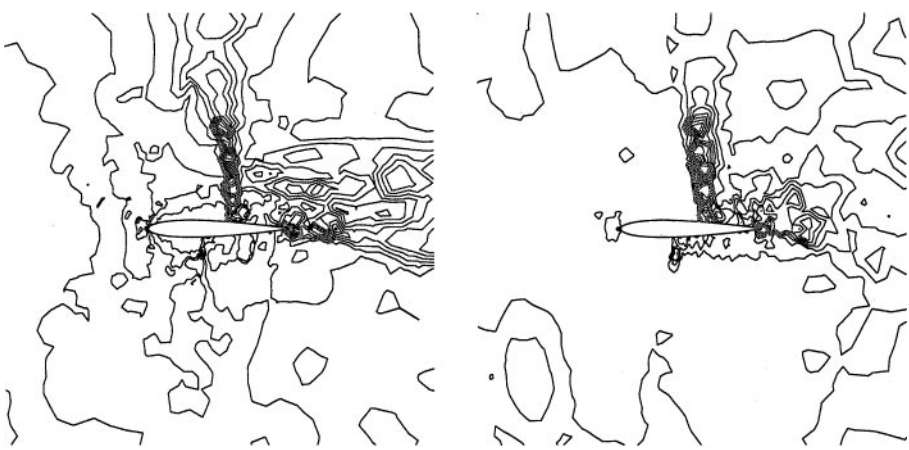

FIG. 11. Left: isolines of H^{-1}-residual estimator. Right: isolines of H^1-residual estimator.

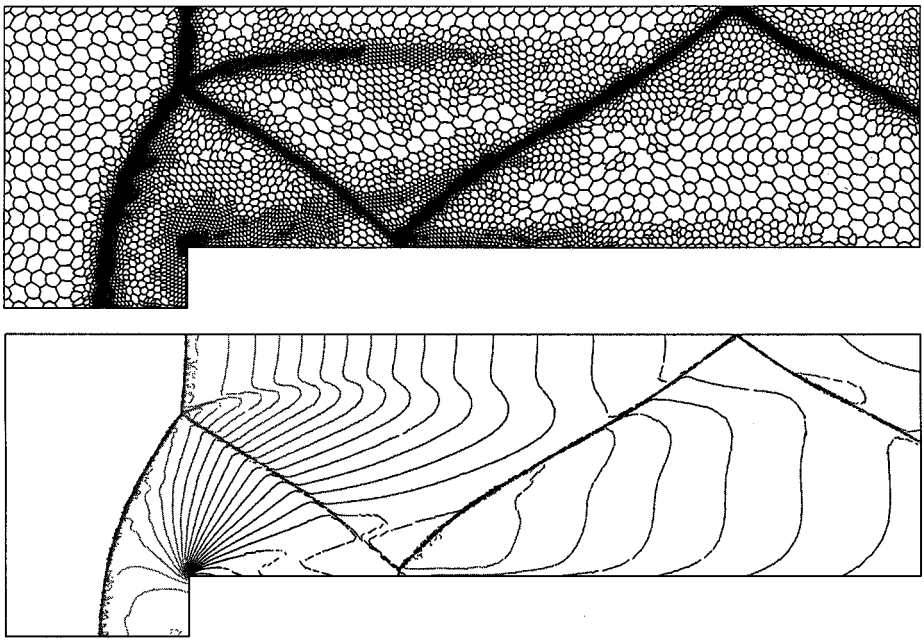

FIG. 12. Grid and density distribution at $t = 8$.

CONCLUSIONS

We have presented a residual estimator based on a certain local smoothness assumption regarding the numerical solution u_h. This assumption allows the use of Taylor series so that the construction of a second order residual estimator is possible. The numerical results showed, in fact, that the new residual indicator behaves very well in comparison with an H^{-1}-indicator with respect to discontinuous solutions. The lack of smoothness in the construction of H^{-1}-indicators seems to lead necessarily to low order devices to indicate regions of error. However, discontinuities take place on lower dimensional manifolds only, so the assumption of low smoothness of the solution everywhere is much too restrictive. On the other hand, a second order piecewise polynomial numerical solution can always be projected onto the space of global H^1-functions while retaining the local order of accuracy in the absence of shocks. Hence we get a higher order residual estimator which guarantees a higher order of convergence in an underlying adaptation process.

REFERENCES

1. O. Friedrich, Weighted essentially nonoscillatory schemes for the interpolation of mean values on unstructured grids, *J. Comput. Phys.* **144**, 194 (1998).
2. O. Friedrich, *Gewichtete Wesentlich Nicht-Oszillierende Verfahren auf Unstrukturierten Gittern* (Ph.D. thesis Universität Hamburg, 1999).
3. C. Hu and C.-W. Shu, Weighted essentially nonoscillatory schemes on triangular meshes, *J. Comput. Phys.* **150**, 97 (1999).
4. T. Sonar, On the construction of essentially nonoscillatory finite volume approximations to hyperbolic conservation laws on general triangulations: polynomial recovery, accuracy, and stencil selection, *Comput. Meth. Appl. Mech. Eng.* **140**, 157 (1997).

5. D. Hempel, *Rekonstruktionsverfahren auf Unstrukturierten Gittern zur Numerischen Simulation von Erhaltungsprinzipien*, Ph.D. thesis (Universität Hamburg, 1999).
6. P. Houston, J. A. Mackenzie, E. Süli, and G. Warnecke, A posteriori error analysis for numerical approximations of Friedrichs systems, *Numer. Math.* **82**, 433 (1999).
7. C. Johnson and A. Szepessy, Adaptive finite element methods for conservation laws based on a posteriori error estimates, *Commun. Pure Appl. Math.* **48**, 199 (1995).
8. T. Sonar, Strong and weak norm refinement indicators based on the finite element residual for compressible flow computation, *Impact Comput. Sci. Eng.* **5**, 111 (1993).
9. T. Sonar, V. Hannemann, and D. Hempel, Dynamic adaptivity and residual control in unsteady compressible flow computation, *Math. Comput. Model.* **20**, 201 (1994).
10. T. Sonar and E. Süli, A dual graph-norm refinement indicator for finite volume approximations of the Euler equations, *Numer. Math.* **78**, 619 (1998).
11. T. Sonar and G. Warnecke, *On Finite Difference Error Indication for Adaptive Approximations of Conservation Laws*, 2nd ed. (Hamburger Beiträge zur Angewandten Mathematik, Universität Hamburg, 1997).
12. T. Sonar and G. Warnecke, On a posteriori error indication based on finite differences in triangular grids, *Z. Angew. Math. Mech.* **78**, Supp. 1, 47 (1998).
13. E. Tadmor, Local error estimates for discontinuous solutions of nonlinear hyperbolic equations, *SIAM J. Numer. Anal.* **28**, 891 (1991).
14. S. Kruzhkov, First-order quasilinear equations in several independent variables, *Mat. Sb.* **123**, 217 (1970).
15. N. Kuznetsow, Accuracy of some approximate methods for computing the weak solutions of a first-order quasilinear equation, *USSR Comput. Math. and Math. Phys.* **16**, 105 (1976).
16. C. Chanais-Hillairet, *Finite Volume Schemes for a Nonlinear Hyperbolic Equation. Convergence Towards the Entropy Solution and Error Estimate*, Tech. Rep., UMPA, E.N.S. Lyon (1997).
17. D. Kröner and M. Ohlberger, A posteriori error estimates for upwind finite volume schemes for nonlinear conservation laws in multi dimensions, *Math. Comput.* **69**, 25 (2000).
18. P. Woodward and P. Colella, The Numerical Simulation of Two-Dimensional Fluid Flow with Strong Shocks, *J. Comput. Phys.* **54**, 115 (1984).